Emission time sequence of neutron and proton as a probe of α-clustering structure*

Bo-Song Huang(黄勃松)[1)] Yu-Gang Ma(马余刚)[2)]

Key Laboratory of Nuclear Physics and Ion-Beam Application (MOE), Institute of Modern Physics, Fudan University, Shanghai 200433, China and Shanghai Institute of Applied Physics, Chinese Academy of Sciences, Shanghai 201800, China

Abstract: Neutron-proton momentum correlation functions are constructed from three-body photodisintegration channel, i.e. $core+n+p$ and used to to explore the spatial-time information of the non-clustering Wood-Saxon spheric structure as well as α-clustering structures of ^{12}C or ^{16}O based on an extended quantum molecular dynamics model. The emission time sequence of neutron and proton is indicated by the ratio of velocity-gated neutron-proton correlation functions, demonstrating its sensitivity to α-clustering structure. The work sheds light on a new probe for α-clustering structure.

DOI:

1 Introduction

High-quality monochromatic photon beams provide a unique way to investigate behaviour of hadrons in nuclear medium [1-5] since photon does not experience strong interaction and can provide useful information about nucleon correlation [6-8]. When photon energy is beyond the giant dipole resonance region which is typically around 15-40 MeV and approaches to 140 MeV, the size of the nucleus is larger than the wavelength of photons which is close to the size of the deuteron. In this energy domain, the quasi-deuteron [QD, a neutron-proton (np) pair inside nucleus] absorption mechanism has been introduced [9], and thus it could provide a unique tool for the study of np correlation. np correlation can be also studied by the two-nucleon knockout reaction in quasi-deuteron region [10-12].

On the other hand, α-clustering state is a significant nuclear structure phenomenon especially in light nuclei, which could be observed at the excited states or even in the ground state. In the evolution of Universe and nuclear synthesis, α particles are involved in the synthesis of ^{12}C and ^{16}O nuclei, and α-clustering structure could emerge inside such nuclei, which is crucial for understanding abundance of elements [13-19]. For nuclei ^{12}C and ^{16}O in the present study, α-clustering structures have been extensively discussed [15]. ^{12}C is of great interest in nuclear astrophysics due to its three-α clustering structure with the Hoyle state [20-29]. ^{16}O has more α-clustering configurations, such as 4-α-clustering chain [30], tetrahedral [31], kite as well as square configurations [32-39]. Of course, many of those configurations are believed to be only emerged in excited states. Some probes have been presented to investigate such clustering structures. For instance, giant resonance photons display corresponding characteristic spectra for different configurations [40-44]. Also, other collective observables show sensitivity to various α-clustering structure during heavy-ion collisions, see eg. Refs. [45-52]. However, these probes are still limited and more probes shall be expected. In this context, here we use the neutron-proton momentum correlation function, especially from different velocity gated correlation functions to investigate the correspondence due to different initial nuclear structure.

In the present work, we applied an Extended Quantum Molecular Dynamics (EQMD) model [53] to simulate photonuclear reaction of ^{12}C and ^{16}O in the quasi-deuteron regime and present a new probe of α-clustering structure by the velocity gated neutron-proton momentum correlation function. With the method of Lednicky and Lyuboshitz (LL) [54], neutron-proton momentum correlation function (C_{np}) can be well constructed through final state three-body decay channel from photodisintegration reaction and emission time sequence

Received 29 May 2020

* This work is partially supported by the National Natural Science Foundation of China under Contracts Nos. 11890714, 11421505, 11905284, and 11961141003, the Strategic Priority Research Program of the CAS under Grants No. XDB34030200 and No. XDB16, and the Key Research Program of Frontier Sciences of the CAS under Grant No. QYZDJ-SSW-SLH002

1) E-mail: huangbosong@sinap.ac.cn

2) E-mail: mayugang@fudan.edu.cn

of neutron and proton could be indicated from the ratio of velocity-gated C_{np}, from which we found that they are sensitive to whether the nuclear configuration is α-clustered or not.

The rest of paper is arranged as follows: in sect. 2, approaches for calculations are introduced, which include brief introductions to the EQMD model, the process of quasi-deuteron absorption as well as the Lednicky and Lyuboshitz's analytical method for momentum correlation. In sect. 3, results and discussion are presented. It contains the model reliability check by the missing energy and recoil momentum, np emission time difference, np momentum correlation function for different α-clustering structures of ^{12}C and ^{16}O and the deduced source sizes with 100 MeV incident photons. Furthermore, emission time sequence of neutron and proton is deduced from the ratio of np correlation functions with different velocity gates between neutron and proton, which demonstrates the sensitivity to whether the nucleus is α-clustered or not. Finally, we summarize the present work in sect. 4.

2 Approaches for calculations

2.1 EQMD model

Quantum molecular dynamics (QMD) model [55, 56] was very successful for dealing with fragmentation in intermediate energy heavy ion collisions [57-59], and EQMD model is one of extension versions of QMD model. In this model, the description of the ground state of the nuclear system has been significantly improved by obtaining the lowest point of energy of the nuclei [53] by the cooling process which cancel the zero-point energy caused by the wave packet broadening in the standard QMD. On the other hand, a Pauli potential is phenomenologically taken into account for treating repulsion between identical nucleons [60]. As a result, saturation property and α-cluster structures can be well obtained after energy cooling in the EQMD model [40, 53]. Different from the traditional QMD model [55, 56], the width of each wave packet in the EQMD model is taken as a dynamical variable [61]. Details can be found in the original paper of Maruyama *et al* [53]. Using the above model, we can obtain different α-clustering structures for ^{12}C and ^{16}O [40] which are taken as target nuclei for photonuclear reactions to perform a detailed study of neutron-proton momentum correlation functions in the present work.

2.2 Process of QD absorption

Photon absorption mechanism plays a dominant role as incident photons are 70 - 140 MeV and a quasi-deuteron (a np pair inside a nucleus) photodisintegration reaction is considered in a process according to Levinger's QD model [62]. The impulse approximation method is applied, where the residue nucleons as spectator besides the correlated np pair after absorbing incident photon energy, and then the nucleus gets excited and experiences transport process to final state, and finally leads to particles' ejection. In this article, three-body decay channel with n + p+ core is only our focus, other decay channels are not discussed here. The phase space information and emission time of protons and neutrons are taken as the input for our correlation calculations using the Lednicky and Lyuboshitz's method which will be briefly introduced later.

In the calculation, for the targets which are composed of N-α clusters, we assume that the incoming photons are randomly distributed in xy-plane, then we choose this event if the incoming photon is inside the region of QD total cross-section. Obviously, the absorbing process will take place in one of α clusters inside target by (γ,^{4}He) for each event. For the process of (γ,^{4}He), we assume the rest two nucleons besides the absorbed quasi-deuteron inside this α-cluster and other clusters in nucleus as the spectators, because spatial separation between the α-clusters is much larger than the pair of quasi-deuteron in the EQMD frame. The kinetic process in our calculation is like that, photon energy transfers to a chosen np pair, and its process is replaced by the reaction of ^{2}H(γ, np). Whether the process occurs or not depends on the total cross section of ^{2}H(γ,np) in each event by the Monte Carlo sampling. Detailed can be found in Ref. [11]. After initial part for the process of (γ, np) has been done, the nucleons could be emitted from the excited nucleus through final state interaction (FSI).

2.3 LL momentum correlation method

Before demonstrating our results, we give a brief description for the momentum correlation calculation using the Lednicky and Lyuboshitz method [54]. Momentum correlation is also known as Hanbury Brown and Twiss (HBT) method [63] which has been extensively applied to the studies of heavy ion collision dynamics [64-69]. The Lednicky and Lyuboshitz method can treat particle-particle correlation functions at small relative momenta which are controlled by particles' quantum-statistical symmetry effects as well as the final-state interaction [70, 71]. Through a square of the symmetrized Bethe-Salpeter amplitude averaged over the emission particles' four coordinates and the total spin of the two-particle system, the correlation function can then be otained. Also, the FSI of the particle pairs is assumed to be independent in the production process. The particle-particle correlation function can be written as

$$\mathbf{C}(\mathbf{k}^*) = \frac{\int \mathbf{S}(\mathbf{r}^*,\mathbf{k}^*)|\Psi_{\mathbf{k}^*}(\mathbf{r}^*)|^2 d^4\mathbf{r}^*}{\int \mathbf{S}(\mathbf{r}^*,\mathbf{k}^*) d^4\mathbf{r}^*}, \quad (1)$$

where $\mathbf{r}^*$ ($=\mathbf{x}_1-\mathbf{x}_2$) and $\mathbf{k}^*$ is the relative distance and half of relative momentum of two particles at kinetic freeze-out, respectively.

3 Results and discussion

3.1 Different initial configurations of ^{12}C and ^{16}O

In this work, we present the calculation of neutron-proton correlation functions for photodisintegration from different initial geometric configurations of ^{12}C and ^{16}O, which are obtained by the process of cooling process in EQMD model. Considering the possible ground state configurations, except for the non-clustering Wood-Saxons (WS) spheric structure, triangle three-α structure for ^{12}C and tetrahedron four-α structure for ^{16}O is the most possible. Of course, from systematic calculation viewpoint, the chain three-α structure for ^{12}C as well as the chain, kite, square four-α structures for ^{16}O can be also available in our model. Even though it is very unlikely for the above α-clustering structures as candidates of ground state configuration, we can still make a complete comparison for observables among all possible configurations in the present calculation. RMS radius and binding energy for different initial nuclei are listed in the first and second columns of Table. 1 and Table. 2 for ^{12}C and ^{16}O, respectively. It is seen that the chain structure which is extremely deformed has the largest RMS radius, while the RMS radius and binding energy for ^{12}C's triangle structure or ^{16}O's tetrahedron one are not so different from the spheric WS distributed nuclei since all these configurations are spatial symmetric. In addition, for ^{16}O, the RMS radius of kite structure is larger than the one of square structure. For the binding energies, they display overall contrary trend among different initial configurations in comparison with the RMS radius cases, which illustrates that larger binding energy makes nucleus more compact.

3.2 Photodisintegration channels

In whole photonuclear reaction simulation in the quasi-deuteron region, there are many different photodisintegration channels, such as two-body channels, three-body channels, and four-body channels and even more channels with very low production probabilities. For three-body channels, we have ^{12}C(γ,np)^{10}B, ^{12}C(γ,pp)^{10}Be, ^{12}C(γ,nn)^{10}C for ^{12}C, and ^{16}O(γ,np)^{14}N, ^{16}O(γ,pp)^{14}C, ^{16}O(γ,nn)^{14}O for ^{16}O. Among all above three-body channels, np channel is overwhelming. In Table 1 and 2, we list branching ratios of three-body np ($B.R._{np}$) and pp ($B.R._{pp}$) channels from our EQMD calculations. For ^{12}C, the $B.R._{np}$ is 92.7%, 90.5% and 52.0%, respectively, for the chain, triangle and sphere configurations. They are significantly larger than 0.45%, 0.75% and 5.05% of $B.R._{pp}$ for the same ^{12}C configurations. For ^{16}O, the $B.R._{np}$ is 89.9%, 90.0%, 89.5%, 89.9% and 60.7%, respectively, for the chain, kite, square, tetrahedron and sphere configurations. They are significantly larger than 0.40%, 0.70%, 0.85%, 1.30%, and 5.13% of $B.R._{pp}$ for the same ^{16}O configurations. In comparison

Table 1. RMS radius (r_{RMS}) of initial configuration, binding energy per nucleon (E_{bind}/A) of initial configuration, average emission time difference between neutron and proton ($\langle\Delta t_{np}\rangle$) and absolute emission time difference between neutron and proton ($|\Delta t_{np}|$) from three-body photodisintegration, HBT radius (R_{pp}) extracted from proton-proton momentum correlation function with 100 MeV photon energy for different ^{12}C configurations [72], the two-proton emission branching ratios ($B.R._{2p}$), HBT radius (R_{np}) extracted from neutron-proton momentum correlation function with 100 MeV photon energy for different ^{12}C configurations, the neutron-proton emission branching ratios ($B.R._{np}$). The experimental data for RMS radius and E_{bind}/A are also shown for the ^{12}C ground state.

Configuration	r_{RMS} (fm)	E_{bind}/A (MeV)	$\langle\Delta t_{np}\rangle$ (fm/c)	$\lvert\Delta t_{np}\rvert$ (fm/c)	R_{pp} (fm)	$B.R._{pp}$	R_{np} (fm)	$B.R._{np}$
Chain	2.71	7.17	1.90	10.13	1.85	0.45%	1.60	92.7%
Triangle	2.35	7.12	1.84	10.85	1.55	0.75%	1.35	90.5%
Sphere	2.23	7.60	0.14	11.32	1.25	5.05%	1.25	52.0%
Exp. Data	2.470 2(22)	7.68						

Table 2. Same as Table I but for ^{16}O configurations.

Configuration	r_{RMS} (fm)	E_{bind}/A (MeV)	$\langle\Delta t_{np}\rangle$ (fm/c)	$\lvert\Delta t_{np}\rvert$ (fm/c)	R_{pp} (fm)	$B.R._{pp}$	R_{np} (fm)	$B.R._{np}$
Chain	3.78	7.26	2.21	11.85	2.40	0.40%	1.80	89.9%
Kite	3.25	7.22	2.01	12.16	1.75	0.70%	1.60	90.0%
Square	2.91	7.29	2.22	12.94	1.60	0.85%	1.55	89.5%
Tetrahedron	2.76	7.79	2.32	13.10	1.50	1.30%	1.40	89.9%
Sphere	2.60	8.15	0.58	11.23	1.40	5.13%	1.45	60.7%
Exp. Data	2.699 1(52)	7.976						

with the non-clustering spheric configuration, np emission channel probabilities are larger for α-clustering structures, which is originated from a favor quasi-deuteron break-up on α-clustering nucleus. As mentioned before, in this work we only focus on three-body channel in final state with core + n + p, which is a dominant photodisintegration process. Their final state phase space information of emitted nucleons is taken as the inputs of the LL model in order to construct the neutron-proton momentum correlation function.

For such a three-body channel, quantitative comparison with the available experimental data is useful to verify the model reliability. Here the recoil momentum spectra of $^{12}C(\gamma,np)^{10}B$ at E $_\gamma$ = 145-157 MeV under the missing energy (E_{miss}) cut less than 40MeV is presented for comparison. By using the distribution of bremsstrahlung with the weight of the $1/E_\gamma$, we can obtain the recoil momentum $\vec{p}_{recoil}=\vec{p}_\gamma-\vec{p}_n-\vec{p}_p$ event by event, where $\vec{p}_\gamma$ is the momentum of incident photons, $\vec{p}_n$ and $\vec{p}_p$ the momentum of emitted protons and neutrons, respectively. E_{miss} can be calculated by $E_\gamma-T_n-T_p-T_{recoil}$, with T_n, T_p and T_{recoil} is defined as kinetic energy of neutron, proton and the recoiled core, respectively. T_{recoil} was obtained from the recoil momentum. In order to compare with the experimental data directly, we scale the count nearly the altitude of the data. From fits to the data, both chain and the triangle three-α clustering structures give similar missing energy distribution with a little higher peak position than experimental main peak. While the spheric structure gives a broad E_{miss} distribution with a lower peak position. For P_{recoil} distribution, the chain configuration gives a wrong peak position, while the triangle and spheric structures have similar peak positions close to the experimental data. Combining with the above E_{miss} and P_{recoil} observables, the triangle α-clustering structure seems to have an overall good agreement with the data, which indicates that it is a very possible ground state configuration for ^{12}C.

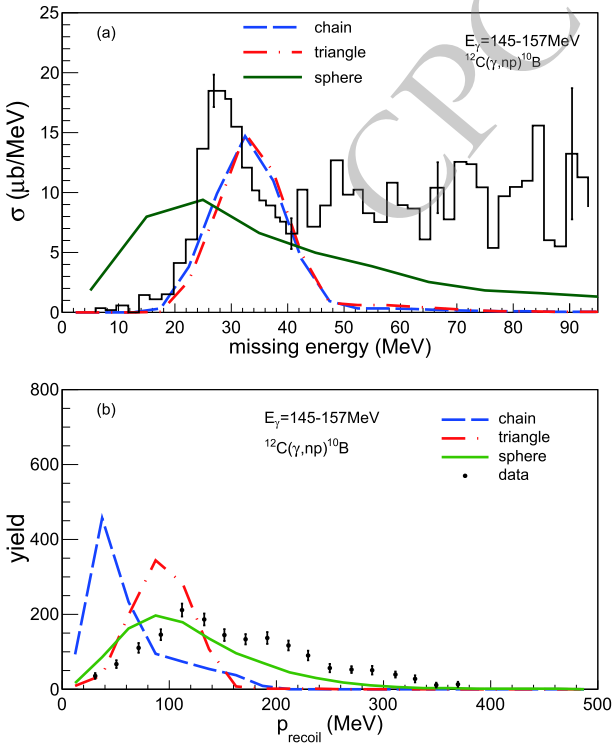

Fig. 1. Comparison of experimental spectra of missing energy (a) and recoil momentum (b) with our model calculations for $^{12}C(\gamma,np)$ at E $_\gamma$ = 145 -157 MeV. Here the same cut of E_{miss} <40 MeV as the data [8] is applied for the calculated P_{recoil}. Different initial geometric configurations of ^{12}C are indicated in the insert.

After the above reliability check of the model, we could further investigate other observables, such as emission time, correlation function as well as emission time sequence of neutron and proton, and try to find a sensitive probe for α-clustering structure which is a main aim of the present work. As an example, we choose 100 MeV photons induced three-body disintegration from ^{12}C and ^{16}O targets in following calculations.

3.3 Difference of np emission time

Difference between emission times of neutron and proton is important for constructing theoretical HBT correlation, especially in a few-body system. The emission time starts from the beginning of photoabsorption. When a deuteron-like pair inside target goes through photon absorption, they obtain additional kinetic energy and then interact with other nucleons. By using a method of coalescence at each time step, the process can be roughly taken as that the rest of target nucleons will remain an entire core after a proton and a neutron are emitted. The emitted proton and neutron can be tracked and the emission time can be obtained, and then using current emission time and phase space information as the inputs for the calculation of correlation functions.

Fig. 2(a) and (b) shows difference of emission time between neutron and proton for different initial ^{12}C as well as ^{16}O configurations, respectively. We can see from Fig. 2(a) that the chain structure with blue dashed line has a sharp peak, while the triangle structure shows a slightly broaden distribution, but both have a higher tail in contrast with the spheric one which is almost symmetric shape. The quantitative time differences ($\langle\Delta t_{np}\rangle = \langle t_n-t_p\rangle$) are listed in Table.1. From the chain, triangle to sphere structures, Δt_{np} corresponds to 1.90, 1.84 and 0.14 fm/c, respectively, which indicates on average proton is emitted earlier than neutron for the photodisintegration from the α-clustering structures, but the sphere case has roughly same emission time sequence between neutron and proton. Here, $\langle\Delta t_{np}\rangle$ is the average over events in which proton is faster than neutron (i.e. $\langle\Delta t_{np}\rangle>0$) and

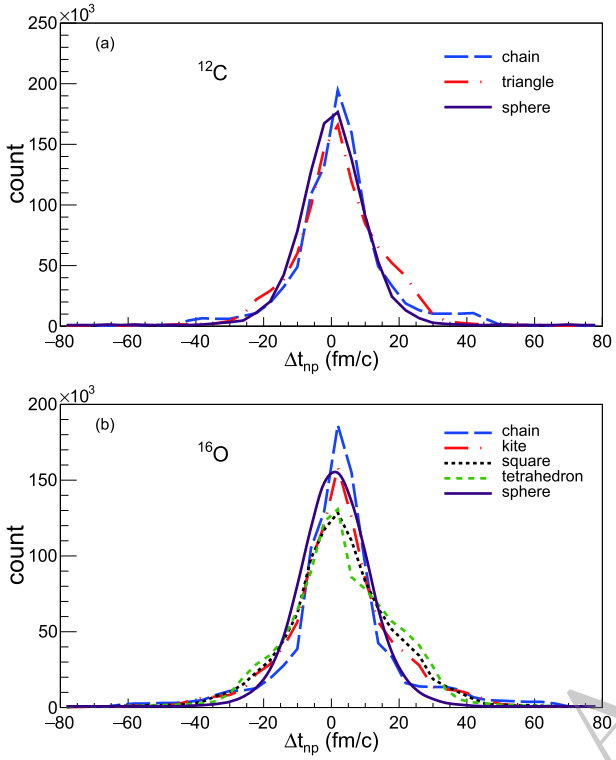

Fig. 2. Difference of emission time between neutron and proton for ^{12}C (a) and ^{16}O (b) with different initial geometric configurations at E_γ = 100 MeV.

events in which proton is slower than neutron (i.e. $\langle\Delta t_{np}\rangle < 0$). A positive value of $\langle\Delta t_{np}\rangle$ indicates that the proton is preferentially emitted earlier than neutron on average. In addition, another quantity is the absolute value $|\Delta t_{np}|$ which is also listed in Table. 1. This value indicates that on average there is around 10-11 fm/c time difference between proton and neutron for ^{12}C photodisintegration without considering who is faster or slower, i.e. there are about half events in which proton is preferentially emitted around 10-11 fm/c earlier than neutron, and about another half events in which neutron is preferentially emitted around 10-11 fm/c earlier than proton.

Similarly, Fig. 2(b) shows the ^{16}O cases with different four α-clustering configurations together with the spheric case, similar situation to ^{12}C is observed. We see the sharpest peak is given by the chain structure, other α-clustering structures are in between, and the most symmetric shape is again from the sphere structure. If we check the values of $\langle\Delta t_{np}\rangle$ as listed in Table. 2, they are 2.21, 2.01, 2.22, 2.32, and 0.58 fm/c, respectively, for the chain, kite, square, tetrahedron and sphere structures. So roughly speaking, all α-clustering configurations make proton preferentially emission earlier but the spheric structure has same emission time sequence between proton and neutron. From $|\Delta t_{np}|$ values for each configuration, they are around rough 11 - 13 fm/c, which is the average time difference between proton and neutron for ^{16}O cases without considering either proton or neutron is faster or slower.

From the above discussion, it seems clean that all α-clustering structures favor earlier proton emission on average but not for the non-clustering spheric structure. However, we should keep in mind that the above emission time sequence and time difference are just taken from the calculation and are not available directly from the experimental measurement. A possible way to access such information experimentally is using the velocity-gated *np* momentum correlation function. In the following texts, we will focus them.

3.4 Neutron-proton momentum correlation function and emission source size

Neutron-proton momentum correlation function can be constructed with the LL model as mentioned above and is presented in Fig. 3(a) and (b), respectively, for photodisintegration channel of ^{12}C(γ,np)^{10}B and ^{16}O(γ,np)^{14}N. Unlike the proton-proton correlation function, there is no Coulomb dip at small relative momentum for neutron-proton correlation function. The order of the correlation strength at a certain small δq, e.g. at 5 MeV/c, follows an increasing trend from the chain, triangle to sphere structure for ^{12}C, while the similar in-

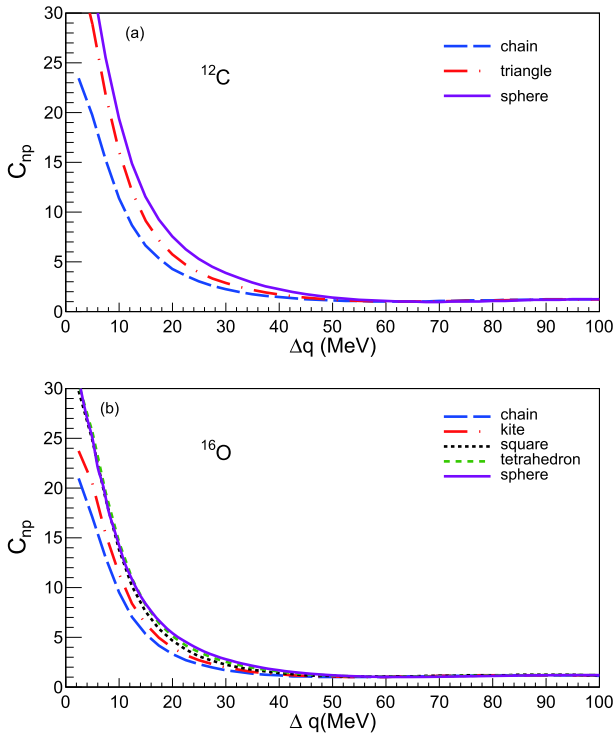

Fig. 3. *np* momentum correlation functions constructed from three-body decay of ^{12}C (a) and ^{16}O (b) at E_γ = 100 MeV. Different initial geometric structures are indicated in the inset.

creasing trend from the chain, kite, square, to tetrahedron or sphere structure for ^{16}O. The reason to explain Fig. 3 could be mainly attributed to the size of different α-clustering configurations, which will be quantitatively extracted in the following texts. Because the chain structure has the largest RMS size, it is then obvious that the correlation function for the chain structure is the weakest. For the triangle structure of ^{12}C and tetrahedron structure of ^{16}O, they have relative stronger correlation strength and close to the spheric case, which indicate that the emission sources are compact and close to the spheric case.

From the above momentum correlation strength, we saw significant difference among various configurations, and interpretation to the source size has been mentioned. To support the above viewpoint, the emission source size was quantitatively determined from the correlation function. As usual, a Gaussian source is assumed for the quantitative estimate of source size from the fits to the HBT correlation results. To do that, the emission time difference between neutron and proton is considered. The space-time dependent Gaussian emission source is written as $\exp\left(-\frac{r^2}{2r_0^2}-\frac{t}{t_0}\right)$, where t_0 is the emission lifetime of the second nucleon under the assumption that the first nucleon is emitted at $t = 0$. t_0 can be given by fitting between t and t', where t is the distribution of emission times of the second nucleon and t' is sampled from an expression of $\exp\left(-\frac{t'}{t_0}\right)$. Through the fit to the np correlation functions, the best fitted source size can be extracted by looking for a minimum of χ^2.

The χ^2 fits to the np correlation functions of different configured ^{12}C (a) and ^{16}O (b) are displayed in Fig. 4. The locations of minimum χ^2 illustrate that the largest source size among the different α-clustering structures is from the chain structure, and the minimum source size is from the triangle structure. The kite and square structures are in middle for ^{16}O. In contrast with clustering structures, the source size for the spheric configuration is the most compact. The order of R_{np} with different configuration is consistent with the initial RMS radii (r_{RMS}) as shown in Table 1 and 2 from which we note that the bigger the space occupancy, the larger the emission source size.

In Table 1 and 2, we also show the HBT radius R_{pp} which was recently extracted from proton-proton correlation function in the same photonuclear reaction [72]. From quantitative point of view, R_{pp} shows a slightly larger value in comparison with R_{np} for α-clustering configurations. The reason is that the neutron-proton pair comes from the same α-cluster while proton-proton pair is not. However, the most important point is that the order of source size R_{pp} versus configurations is exactly the same as R_{np}.

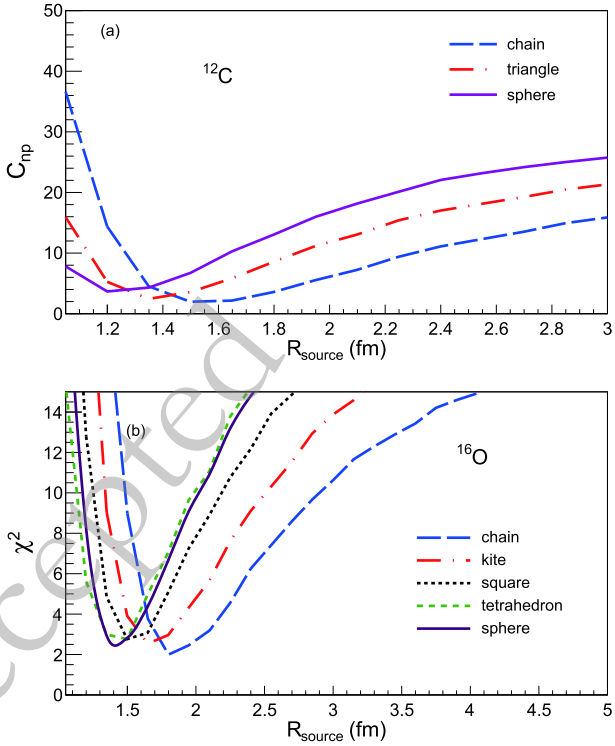

Fig. 4. χ^2 fits to C_{np} of Fig. 3. The minimum points represent the best fitted values of the deduced source sizes which are listed in Table. I and II as R_{np}.

3.5 np emission time sequence

In contrast with the identical particle correlation, the velocity-gated correlation functions for non-identical particles can give the emission chronology information of the particles [74-78]. Since we are treating neutron and proton, emission time sequence could be deduced from the velocity-gated momentum correlation functions.

Fig. 5 shows the ratio between C_n and C_p for different configurations of ^{12}C and ^{16}O, where the correlation function C_n represents C_{np} gated on the velocity cuts with $v_n > v_p$, i.e. velocity of emitted neutron is faster than that of proton, while C_p represents C_{np} under the cut of $v_n < v_p$, i.e. emitted neutron is slower than emitted proton. The ratio is defined by comparing the above velocity-gated correlation functions, i.e. C_n/C_p. By investigating C_n/C_p, we could obtain the emission time sequence in nuclear collisions by a basic ideal as following: if one particle has lower velocity and is emitted earlier, it will travel a shorter distance before another particle is emitted, and vice versa.

If proton is on average emitted earlier than neutron, the ratio C_n/C_p would show a dip in the region of stronger correlation, otherwise there exists a peak correspondingly [74]. Interestingly, dips in $\Delta q \approx 20$ MeV/c which is the region of np strong interaction is observed for all α-clustering configurations of ^{12}C and ^{16}O. It

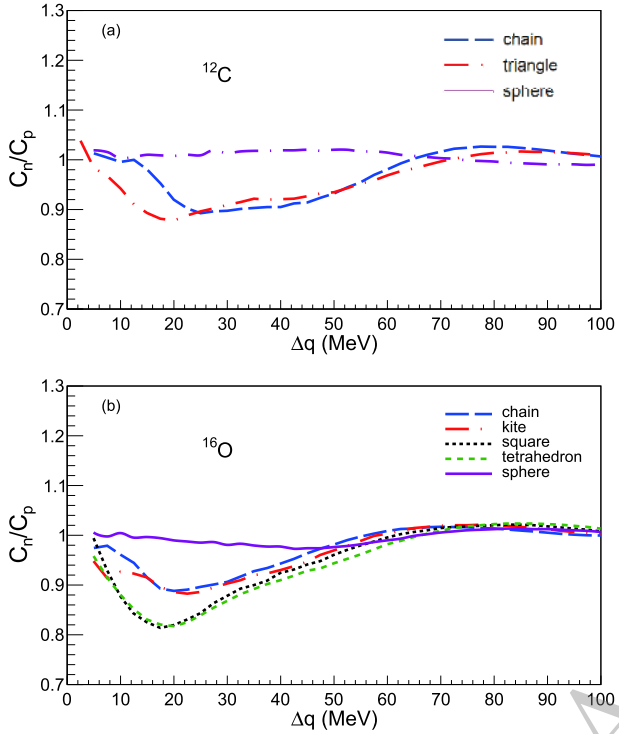

Fig. 5. Ratio of correlation functions between C_n and C_p where C_n represents C_{np} gated with $v_n > v_p$ and C_p represents C_{np} gated with for $v_n < v_p$ for 100 MeV induced three-body photodisintegration of ^{12}C (a) and ^{16}O (b). Different initial geometric configurations are indicated in the insert.

means that proton is emitted earlier than neutron on average for photodisintegration from α-clustering nuclei, which is consistent with the scenario depicted in Fig. 2, i.e. $\Delta_{np} > 0$. For different α-clustering configurations, we observe that the triangle case has a little deeper and narrower dip than the chain case for ^{12}C, which is consistent with a little larger Δt_{np} value for the chain structure. Very different from the α-clustering cases, C_n/C_p for the spheric structure is almost flat, which indicates the nearly same emission sequence for proton and neutron on average, which is consistent with negelectable Δt_{np} values in Table. 1.

For ^{16}O cases, the width and depth of C_n/C_p for the tetrahedron and square cases are almost the same, and both are deeper than the chain and kite cases, which indicates that in all α-clustering cases the emitted proton is on average faster than emitted neutron, and proton is a little faster for the square and the tetrahedron cases in contrast with the chain and kite cases, which is also represented by the largest values of Δt_{np}. For the spheric case, an almost flat C_n/C_p distribution reflects that neither proton and nor neutron have priority emission order, which is consistent with the smallest Δt_{np} value listed in Table 2.

Based upon the above C_n/C_p as a function of Δ q and deduced emission time sequence, we found that the α-clustering structures, regardless the ground state or excited state configuration candidates of ^{12}C and ^{16}O, could be well distinguished from the non-clustering spheric WS structure. This is a very interesting and important conclusion. From the experimental point of view, such measurement is feasible in near future. Therefore, it is proposed that the velocity gated np correlation function can be taken as a good probe of α-clustering structure. The reason of the above different np emission time sequence between the α-clustering structures and the non-clustering spheric WS structure might be understood by the stronger Coulomb repulsion for protons inside α-cluster than those inside the spheric non-clustered nucleus, and the former makes proton acceleration easily.

4 Summary

The process of quasi-deuteron photoabsorption around 100 MeV photon energy is investigated in a framework of an extended quantum molecular dynamics model, and np momentum correlation functions are investigated from three-body photodisintegration channels from ^{12}C and ^{16}O systems which are considered by different α-clustering structures or non-clustering Wood-Saxon structures. The np momentum correlation function and deduced source size show dependence of initial structures in some extents. However, more interesting point is that the ratio of the np correlation functions gated by $v_n > v_p$ and $v_n < v_p$ reveal the sensitivity to α-clustering structure, i.e. broad dips around $\Delta q \simeq 20$ MeV/c are demonstrated for all α-clustering structures but not for the spheric Wood-Saxon nucleon distribution. It indicates that the neutron is on average emitted later than the proton in photodisintegration from α-clustering nuclei, but neither proton nor neutron has prior emission time sequence on average for the non-clustering spheric structure. This is an interesting probe for α-clustering structure regardless of ground-state or excited-state α-clustering candidates of ^{12}C and ^{16}O from the present systematic calculation. Even though no experimental data available for such three-body photodisintegration channel so far, it is expected to perform such photonuclear reactions in near-future photon factories, and then velocity-gated np momentum correlation functions could be measured, which will shed light on nuclear clustering structure information.

On the other hand, the present EQMD model might be further improved by introducing high momentum tails of neutrons and protons stemming from short-range correlation (SRC) [79], and then may lead to observable effects on the momentum correlations of np, nn and pp pairs. By careful comparisons of different nucleon-nucleon pairs w/ and w/o SRC especially from different α-

clustering structure, it could highlight information of SRC specifically for α-conjugate nuclei.

References

1 O. A. P. Tavares, S. B. Duarte, A. Deppman *et al*.., J. Phys. G, **30**: 377 (2004)
2 H. R. Weller, A. W. Mohammad, H. Gao *et al*.., Prog. Part. Nucl. Phys., **62**: 257 (2009)
3 D. Filipescu, A. Anzalone, D. L. Balabanski *et al*.., Eur. Phys. J. A, **51**: 185 (2015)
4 J. W. Wang, G. T. Fan, H. W. Wang *et al*.., Nucl. Tech. (in Chinese), **42**: 120201 (2019)
5 S. Amano, K. Horikawa, K. Ishihara *et al*.., Nucl. Inst. Meth. A, **602**: 337 (2009)
6 J. C. McGeorge, I. J. D. MacGregor, S. N. Dancer *et al*.., Phys. Rev. C, **51**: 1967 (1995)
7 I. J. D. MacGregor *et al*.., Nucl. Phys. A, **533**: 269 (1991)
8 I. J. D. MacGregor, SciPost Physics Proceedings; 24th European Few Body Conference (University of Surrey, U.K.).
9 J. S. Levinger, Phys. Rev., **84**: 43 (1951)
10 E. C. Sympson and J. A. Tostevin, Phys. Rev. C, **83**: 014605 (2011)
11 B. S. Huang, Y. G. Ma, W. B. He, Phys. Rev. C, **95**: 034606 (2017)
12 B. S. Huang, Y. G. Ma, W. B. He, Eur. Phys. A, **53**: 119 (2017)
13 K. Ikeda, N. Takigawa, and H. Horiuchi, Prog. Theor. Phys. Suppl. E, **68**: 464 (1968)
14 Y. Fujiwara, Y. Suzuki, H. Horiuchi, K. Ikeda, M. Kamimura, K. Kato, Y. Suzuki, and E. Uegaki, Prog. Theor. Phys. Suppl., **68**: 29 (1980)
15 W. von Oertzen, M. Freer, and Y. Kanada-Enyo, Phys. Rep., **432**: 43 (2006)
16 A. Tohsaki, H. Horiuchi, P. Schuck, and G. Röpke, Phys. Rev. Lett., **87**: 192501 (2001)
17 M. Freer, Rep. Prog. Phys., **70**: 2149 (2007)
18 M. Freer, H. Horiuchi, Y. Kanada-En 'yo, D. Lee, and Ulf-G. Meißner, Rev. Mod. Phys., **90**: 035004 (2018)
19 J.-P. Ebran, E. Khan, T. Niksic, and D. Vretenar, Nature (London), **487**: 341 (2012)
20 E. M. Burbidge, G. R. Burbidge, W. A. Fowler, F. Hoyle, Rev. Mod. Phys., **29**: 547 (1957)
21 F. Hoyle, Astrophys. J. Suppl. Ser., **1**: 121 (1954)
22 H. Fynbo, C. A. Diget, U. C. Bergmann *et al*.., Nature, **433**: 136 (2005)
23 Wei Liu, Jian-Ling Lou, Yan-Lin Ye, Dan-Yang Pang, Nucl. Sci. Tech., **31**: 20 (2020)
24 H. Pais, F. Gulminelli, C. Providencia, G. Röpke, Nucl. Sci. Tech., **29**: 181 (2018)
25 X. D. Tang, S. B. Ma, X. Fang, B. Bucher, A. Alongi, C. Cahillane, W.-P. Tan, Nucl. Sci. Tech., **30**: 126 (2019)
26 Y. P. Shen, B. Guo, R. J. deBoer *et al*.., Phys. Rev. Lett., **124**: 162701 (2020)
27 S. Zhang, J. C. Wang, A. Bonasera *et al*.., Chin. Phys. C, **43**: 064102 (2019)
28 W. J. Li, Y. G. Ma, G. Q. Zhang *et al*.., Nucl. Sci. Tech., **30**: 180 (2019)
29 Z. X. Ren, P. W. Zhao, J. Meng, Phys. Lett., **801**: 135194 (2020)
30 T. Ichikawa, J. A. Maruhn, N. Itagaki *et al*.., Phys. Rev. Lett., **107**: 112501 (2011)
31 T. Suhara, Y. Funaki, B. Zhou *et al*.., Phys. Rev. Lett., **112**: 062501 (2014)
32 M. Girod and P. Schuck, Phys. Rev. Lett., **111**: 132503 (2013)
33 E. Epelbaum, H. Krebs, D. Lee, and Ulf-G. Meißner, Phys. Rev. Lett., **106**: 192501 (2011)
34 E. Epelbaum, H. Krebs, T. A. Lähde, D. Lee, Ulf-G. Meißner, and G. Rupak, Phys. Rev. Lett., **112**: 102501 (2014)
35 D. J. Marn-Lmbarri, R. Bijker, M. Freer, M. Gai, Tz. Kokalova, D. J. Parker, and C. Wheldon, Phys. Rev. Lett., **113**: 012502 (2014)
36 Bo Zhou, Y. Funaki, H. Horiuchi, Zhongzhou Ren, G. Röpke, P. Schuck, A. Tohsaki, Chang Xu, and T. Yamada, Phys. Rev. Lett., **110**: 262501 (2013)
37 X. G. Cao, E. J. Kim, K. Schmidt *et al*.., Phys. Rev. C, **99**: 014606 (2019)
38 Y. Liu and Y. L. Ye, Nucl. Sci. Tech., **29**: 184 (2018)
39 X. B. Wang, G. X. Dong, Z. C. Gao *et al*.., Phys. Lett. B, **790**: 498 (2019)
40 W. B. He, Y. G. Ma, X. G. Cao, X. Z. Cai and G. Q. Zhang, Phys. Rev. Lett., **113**: 032506 (2014)
41 Y. Kanada-En 'yo and K. Ogata, Phys. Rev. C, **101**: 014317 (2020)
42 T. Yamagata, S. Nakayama, H. Akimune, and S. Miyamoto, Phys. Rev. C, **95**: 044307 (2017)
43 Y. Kanada-En'yo, Phys. Rev. C, **93**: 024322 (2016)
44 Z. H. Yang, Y. L.Ye, Z. H. Li *et al*.., Phys. Rev. Lett., **112**: 162501 (2014)
45 W. Broniowski and E. Ruiz Arriola, Phys. Rev. Lett., **112**: 112501 (2014)
46 P. Bozek, W. Broniowski, E. Ruiz Arriola, and M. Rybczynski, Phys. Rev. C, **90**: 064902 (2014)
47 C. C. Guo, Y. G. Ma, Z. D. An, and B. S. Huang, Phys. Rev. C, **99**: 044607 (2019)
48 S. Zhang, Y. G. Ma, J. H. Chen, W. B. He, C. Zhong, Phys. Rev. C, **95**: 064904 (2017)
49 S. Zhang, Y.G. Ma, J. H. Chen, W.B. He and C. Zhong, Eur. Phys. J. A, **54**: 161 (2018)
50 Zhi-Wan Xu, Song Zhang, Yu-Gang Ma, Jin-Hui Chen, Chen Zhong, Nucl. Sci. Tech., **29**: 186 (2018)
51 Yi-Lin Cheng, Song Zhang, Yu-Gang Ma, Jin-Hui Chen, and Chen Zhong, Phys. Rev. C, **99**: 054906 (2019)
52 J. J. He, S. Zhang, Y. G. Ma, J. H. Chen, C. Zhong, Eur. Phys. J. A, **56**: 52 (2020)
53 T. Marayama, K. Niita, A. Iwamoto, Phys. Rev. C, **53**: 297 (1996)
54 R. Lednicky, Sov. J. Nucl. Phys., **35**: 770 (1982)
55 J. Aichelin, H. Stocker, Phys. Lett. B, **176**: 14 (1986)
56 J. Aichelin, Phys. Rep., **202**: 233 (1991)
57 C. Hartnack, R. K. Puri, J. Aichelin *et al*.., Eur. Phys. J. A, **1**: 151 (1998)
58 C. Hartnack, Zhuxia Li, L. Neise *et al*.., Nucl. Phys. A, **495**: 303 (1989)
59 Z. Q. Feng, Nucl. Sci. Tech., **29**: 40 (2018)
60 A. Ohnishi, T. Maruyama, H. Horiuchi, Prog. Theor. Phys., **87**: 417 (1992)
61 P. Valta, J. Konopka, A. Bohnet *et al*.., Nucl. Phys. A, **538**: 417 (1992)
62 J. S. Levinger, Phys. Lett. B, **82**: 181 (1979)
63 R. Hanbury Brown, R. Q. Twiss, Nature, **178**: 1046 (1956)
64 F. M. Marques, M. Labiche, N. A. Orr *et al*.., Phys. Rev. C, **64**: 061301 (2001)
65 L. W. Chen, V. Greco, C. M. Ko, B. A. Li, Phys. Rev. Lett., **90**: 162701 (2003)
66 Y. G. Ma, Y. B. Wei, W. Q. Shen *et al*.., Phys. Rev. C, **73**: 014604 (2006)
67 X. G. Cao, Y. G. Ma, D. Q. Fang *et al*.., Phys. Rev. C, **86**: 044620 (2012)
68 D. Q. Fang, Y. G. Ma, X. Y. Sun *et al*.., Phys. Rev. C, **94**: 044621 (2016)
69 T. T. Wang, Y. G. Ma, C. J. Zhang, Z. Q. Zhang, Phys. Rev. C, **97**: 034617 (2018)

70 S. E. Koonin, Phys. Lett. B, **70**: 43 (1977)
71 S. Pratt and M. B. Tsang, Phys. Rev. C, **36**: 2390 (1987)
72 B. S. Huang and Y. G. Ma, Phys. Rev. C, **101**: 034615 (2020)
73 L. Adamczyk *et al*.., Nature, **527**: 345 (2015)
74 R. Lednicky, V.L. Lyuboshitz, B. Eranmus, D. Nouais, Phys. Lett. B, **373**: 30 (1996)
75 C. J. Gelderloos *et al*.., Phys. Rev. Lett., **75**: 3082 (1995)
76 S. Voloshin, R. Lednický, S. Panitkin, and Nu Xu, Phys. Rev. Lett., **79**: 4766 (1997)
77 R. Ghetti *et al*.., Phys. Rev. Lett., **87**: 102701 (2001)
78 T. T. Wang, Y. G. Ma, Z. Q. Zhang, Phys. Rev. C, **99**: 054626 (2019)
79 R. Subedi *et al*.., Science, **320**: 1476 (2008)